Int J Clin Exp Med 2015;8(2):1726-1736
www.ijcem.com /ISSN:1940-5901/IJCEM0004940

Original Article

Detection of pulmonary metastases with the novel radiolabeled molecular probe, ^{99m}Tc-RRL

Ning Yao[1], Ping Yan[1], Rong-Fu Wang[1], Chun-Li Zhang[1], Chao Ma[1], Xue-Qi Chen[1], Qian Zhao[2], Pan Hao[1]

[1]*Department of Nuclear Medicine, Peking University First Hospital, West District, Beijing 100034, China;*
[2]*Department of Nuclear Medicine, General Hospital of Ningxia Medical University, Xingqing District, Yinchuan 750004, Ningxia, China*

Received December 16, 2014; Accepted February 12, 2015; Epub February 15, 2015; Published February 28, 2015

Abstract: Background: To improve the detection of pulmonary metastases, experimental blood-borne pulmonary metastasis mouse models were established using three intravenously administered cell lines. In a previous study we demonstrated that ^{99m}Tc-radiolabeled arginine-arginine-leucine (RRL) could be used to non-invasively image malignant tumors. Methods: ^{99m}Tc-RRL was prepared and injected intravenously in mice with pulmonary metastases that arose from the intravenous injection of HepG2, B16, and Hela cells. The bio-distribution and imaging of ^{99m}Tc-RRL were determined in different pulmonary metastases mouse models and in normal mice. Results: ^{99m}Tc-RRL exhibited higher uptake values in the lungs of pulmonary metastatic mice compared to normal mice ($P<0.05$; 3.92±0.48% ID/g 2 h post-injection and 3.89±0.36% ID/g 4 h post-injection in metastatic hepatic carcinoma [HepG2]-bearing lungs; 5.49±0.84% ID/g 2 h post-injection and 5.11±0.75% ID/g 4 h post-injection in metastatic melanoma [B16]-bearing lungs; 3.72±0.52% ID/g 2 h post-injection and 3.51±0.35% ID/g 4 h post-injection in metastatic cervical carcinoma [Hela]-bearing lungs; 2.38±0.20% ID/g 2 h post-injection and 2.11±0.24% ID/g 4 h post-injection in normal lungs). The pulmonary metastatic lesions were clearly visualized using ^{99m}Tc-RRL. Conclusions: ^{99m}Tc-RRL exhibited favorable metastatic tumor targeting and imaging properties, thus highlighting its potential as an effective imaging probe for detection of pulmonary metastases. ^{99m}Tc-RRL can be used as a reasonable supplement to ^{18}F-FDG imaging in the non-invasive imaging of tumor angiogenesis.

Keywords: ^{99m}Tc, peptide, tumor angiogenesis, lung metastasis, non-invasive imaging

Introduction

Cancer incurs tremendous economic burden and mental anguish in the affected. At present, the types of cancer that occur in different regions and countries fluctuate slightly, but there is no reduction in the number of cancer patients [1]. Although it would be ideal to diagnose cancer as early as possible, the unfortunate fact is that most cancers are still diagnosed and treated at an advanced stage. Molecular functional imaging can systematically evaluate cancer patients and be used to effectively diagnose the number and staging of primary tumors and metastases, which can in turn provide information for the management of cancer patients [2-5].

Metastasis is the late stage of tumor angiogenesis and the major cause of death in cancer patients. Therefore, detecting tumor metastasis is receiving more attention [6-10]. Metastasis is a complex and multistep process in which cancer cells not only invade the surrounding tissues and translocate through the blood stream to capillaries of distant tissues, but also survive in blood and adjust to the microenvironment before proliferating and forming tumor metastases [11]. Tumor angiogenesis is very important in the growth and metastasis of malignant tumors. Tumor cell survival and amplification in metastatic sites requires induction of angiogenesis. Therefore, angiogenesis is essential for the initiation as well as development of metastases [12, 13]. Recently, reporter-based visualization of cancer cell migration during the metastatic process has been reported in many publications, but few studies have imaged distant metastases using radiolabeled probes.

Table 1. Radio frequency (Rf) values (two kinds of developing solvent)

Immobile Phase	Mobile Phase	Rf		
		$^{99m}TcO_4^-$	$^{99m}TcO_2.nH_2O$	^{99m}Tc-RRL
Xinhua no. 1 filter paper	Ethanol: Ammonia: Water (2:1:5)	0.9~1.0	0~0.1	0.8~1.0
	Acetone	0.9~1.0	0~0.1	0~0.1

Table shows radio frequency values of the various radio labeled compounds as measured using a radioactivity meter.

The most common agent used for imaging tumors, ^{18}F-FDG, is not tumor-specific and accumulates in areas where glucose metabolism is increased. For example, ^{18}F-FDG uptake is often masked by surrounding inflammatory changes [14-17], and ^{18}F-FDG shows high physiologic uptake in brain and heart tissues [18, 19]. Detection of tumor growth and metastasis using a probe that specifically targets tumor-induced angiogenesis is a promising direction for new molecular imaging modalities [29, 30]. Brown [21] first identified a tumor vasculature-specific binding peptide (RRL) from a phage peptide display library. *In vitro* binding experiments with tumor-derived epithelial cells (TDECs) were carried out. Fluorescein FITC-labeled RRL peptide had the brightest staining and specificity for TDECs. Gregory [22] conjugated microbubbles (MBs) to RRL via avidin/biotin bridging chemistry. MBs were successfully targeted to tumor-derived cells, but not normal endothelial cells to aid in tumor imaging. Our earlier study demonstrated that RRL targeted neovascularization [24]. Previously, we redesigned, radiolabeled, and imaged a novel ^{99m}Tc-labeled RRL and demonstrated that this new molecular probe has the potential for imaging tumor angiogenesis in malignant liver carcinoma [20]. In the current study we tested the ability of this imaging agent to detect pulmonary metastases in three different metastatic models and determined whether or not ^{99m}Tc-RRL imaging could be effective in tumor xenografts and metastases models. We also determined whether or not ^{99m}Tc-RRL could be used as a supplement to ^{18}F-FDG imaging in the non-invasive imaging of tumor angiogenesis.

Materials and methods

Ethics statement

Our study was conducted in rigorous compliance with official recommendations. All animal experiments were approved by the authority of Peking University Animal Studies Committee in accordance with the Guidelines for the Care and Use of Research Animals (Peking University, China) (Approval ID: J201312). Mice were housed and maintained in a specific pathogen-free colony using standard bedding, diet, and environment with free access to food and drinking water according to the guidelines. Mice were sacrificed by cervical dislocation under anesthesia (to minimize suffering).

Radiosynthesis and purification of ^{99m}Tc-RRL

Before the experiments were performed, 0.2 M ammonium acetate buffer was prepared and RRL (50 μg) was dissolved in phosphate buffer (PB; 50 μL of 0.5 M [pH 7.4]). Fresh $SnCl_2$ solution (0.25 mg/mL) was dissolved in 50 mM hydrochloric acid (HCl), and sodium tartrate (10 mg/mL) was prepared just prior to use. The fresh ^{99m}Tc-pertechnetate elute was obtained from a ^{99}Mo-^{99m}Tc radionuclide generator (China Institute of Atom Energy, Beijing, China). Radiosynthesis was performed as previously described [20]. Briefly, RRL was radiolabeled using a one-step method. At room temperature, 7.4 MBq ^{99m}TcO4-eluant (50 μL) was added to 50 μL of $SnCl_2$ solution, 100 μL of ammonium acetate buffer, and 50 μL of RRL.

After 60 min, the labeled product was purified on a Sephadex G25 gel filtration column with 0.05M PB (pH 7.4) as the eluent. The gel filtration column first eluted with 1% bovine serum albumin, and eluted with phosphate-buffered saline (PBS, 0.05 M [pH 7.4]). The radioactivity of all fractions was detected with radioactivity meters (National Institute of Metrology, Beijing, China). To control the quality of labeling, double-phase paper chromatography (Xinhua no. 1 filter paper; Beijing Safelab Technology Ltd, Beijing, China) was performed to measure labeling efficiency and radiochemical purity (**Table 1**). The mobile phase was acetone and ethanol: ammonia: water (2:1:5).

Cell lines and reagents

All cell lines used in this study were generous gifts from the Department of Pathology of

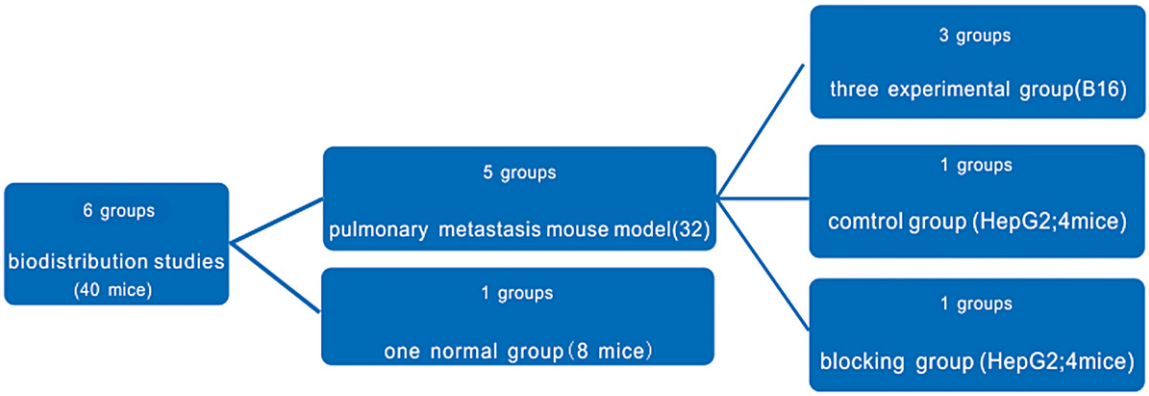

Figure 1. Schematic of groups analyzed for biodistribution. Forty BALB/c nu/nu mice were used in this study. There was one normal group, which was not implanted with any cancer cells. The other five groups (three experimental groups, one blocking group, and one control group) were injected with different cell lines. The experimental groups consisted of one pulmonary metastases HepG2-bearing group, one pulmonary metastases Hela-bearing group, and one pulmonary metastases B16/F10-bearing group. The blocking and control groups were both planted with HepG2. Three experimental groups and one normal group consisting of eight mice were divided into two subgroups of four mice each.

Peking University First Hospital, and were maintained in the recommended media. The tumor cell lines included the human HepG2 hepatocellular carcinoma cell line (ATCC No. HB-8065; [Rockefeller, Maryland, USA]), the human Hela cervical cancer line (ATCC No. CCL-2), and the mouse B16/F10 melanoma cell line (ATCC CRL No. 6322). HepG2 and Hela cells were cultured in Dulbecco's modified Eagle medium (DMEM)/high glucose medium containing 10% fetal bovine serum (Invitrogen; [New York, New York State, USA]), 2 mmol/L glutamine, and 4500 mg/L glucose. B16 cells were cultured in RPMI-1640 medium supplemented with 10% fetal bovine serum and 1 mmol/L glutamine. All commercially available chemical reagents were used without further purification. All cells were grown at 37°C in a humidified atmosphere containing 95% air and 5% CO_2. The cell growth status was visualized by inverted microscopy with phase contrast (Olympus, Tokyo, Japan), and the cells were used in the logarithmic phase of growth.

Biodistribution

All animal studies complied with the Guidelines for the Care and Use of Research Animals established by the Peking University Animal Studies Committee. BALB/c nu/nu female mice (20±3 g, 3-4 weeks old; Department of Laboratory Animal Science, Peking University First Hospital) were used in this study. The human HepG2 cell line, the human Hela cervical cancer line, and the mouse B16 melanoma cell line were used to simulate pulmonary metastases. Pulmonary metastases models were generated by injecting 1×10^6 HepG2 cells, Hela cells, or B16/F10 cells into BALB/c nu/nu mice through the tail vein. All pulmonary metastases mice were used for bio-distribution studies 8 weeks after the injection of cells. The mice were housed and maintained in a SPF colony. The bio-distribution studies for female mice were performed as follows.

Forty BALB/c nu/nu mice (6 groups) were used in this study (**Figure 1**). There was one normal group, which was not implanted with any cancer cells. The other 5 groups (3 experimental groups, 1 blocking group, and 1 control group) were injected with different cell lines as described above. The experimental groups consisted of 1 pulmonary metastasis HepG2-bearing group, 1 pulmonary metastasis Hela-bearing group, and 1 pulmonary metastasis B16/F10-bearing group. The blocking and control groups were both implanted with HepG2 cells. Three experimental groups and 1 normal group containing 8 mice were divided into 2 subgroups of 4 mice each. The three experimental groups were treated with ^{99m}Tc-RRL, and the control group was only administered Na ^{99m}TcO4. The blocking group was treated with unlabeled RRL (500 mg dissolved in 50 mL of 0.5M PB [pH = 7.4]) from the lateral tail vein 30 minutes before injection of ^{99m}Tc-RRL.

The three experimental groups and one normal group were treated with ^{99m}Tc-RRL as follows. A single dose of 1,850 kBq of ^{99m}Tc-RRL was injected into each mouse via the lateral tail

Table 2. Biodistribution of ^{99m}Tc-RRL in HepG2, B16, and Hela pulmonary metastases and normal mice

	% ID/g							
	2 h				4 h			
	Lung metastases			Normal	Lung metastases			Normal
Tissue	HepG2	B16	Hela		HepG2	B16	Hela	
Heart	1.60±0.07	1.66±0.11	1.68±0.07	1.70±0.05	1.44±0.09	1.47±0.08	1.44±0.07	1.55±0.07
Liver	1.40±0.06	1.38±0.06	1.38±0.12	1.30±0.07	1.22±0.09	1.26±0.13	1.33±0.08	1.23±0.08
Spleen	1.06±0.10	1.01±0.22	1.13±0.16	1.09±0.19	1.03±0.03	0.93±0.06	0.98±0.10	1.06±0.09
Lung	3.92±0.48*	5.49±0.84*	3.72±0.52*	2.38±0.20	3.89±0.36*	5.11±0.75*	3.51±0.35*	2.11±0.24
Kidney	9.05±0.59	9.15±0.81	9.23±0.87	8.18±0.50	7.57±0.39	7.99±0.89	7.94±0.70	7.30±0.48
Bone	3.61±0.57	3.60±0.29	3.86±0.45	3.34±0.38	3.04±0.19	3.21±0.38	2.99±0.45	3.21±0.36
Stomach	9.01±0.52	9.81±0.46	8.82±0.44	9.51±0.40	8.06±0.67	8.27±0.85	7.89±1.16	8.02±0.65
Muscle	0.60±0.05	0.59±0.10	0.57±0.08	0.56±0.07	0.49±0.06	0.55±0.09	0.42±0.07	0.51±0.08
Intestine	1.65±0.23	1.43±0.11	1.77±0.23	1.64±0.14	1.21±0.25	1.06±0.13	1.02±0.22	1.30±0.17
Bladder	2.76±0.39	2.65±0.36	3.11±0.66	3.03±0.46	2.52±0.35	2.40±0.25	2.24±0.23	2.49±0.28
Blood	2.08±0.15	2.07±0.14	2.15±0.11	2.09±0.18	1.43±0.14	1.42±0.13	1.56±0.14	1.48±0.20
	Uptake rate of tumor/normal tissue							
Lung/heart	2.45	3.31	2.21	1.40	2.70	3.48	2.14	1.36
Lung/kidney	0.43	0.60	0.40	0.29	0.51	0.64	0.44	0.29
Lung/blood	1.88	2.64	1.73	1.14	2.72	3.57	2.25	1.43
Lung/muscle	6.53	9.31	6.52	4.25	7.94	9.28	8.36	4.14
	Uptake rate of tumor-bearing lung/normal lung (TL/NL)							
TL/NL	1.65	2.31	1.56		1.84	2.42	1.66	

*P<0.05, significant differences among levels of ^{99m}Tc-RRL in HepG2, B16, and the Hela pulmonary metastases mouse model and the ^{99m}Tc-RRL normal mouse model. The experimental data were analyzed with single factor analysis of variance (one-way ANOVA), Means in multiple samples were compared between two groups of completely randomized design, and it was deduced whether the overall means of two groups of data are equal. Data are presented as the % ID/g (mean ± SD; n = 4).

vein. Groups of 4 mice per time point were sacrificed at 2 or 4 h after injection for the bio-distribution studies. The organs of interest (heart, liver, spleen, lung, kidney, bone, stomach, muscle, intestine, urine, and blood) were harvested, weighed, and counted. The results are expressed as the percentage injected activity per gram (% ID/g) of tissue, corrected for background and decay.

Imaging of pulmonary metastatic tumors with ^{99m}Tc-RRL

Fifteen BALB/c nu/nu mice with pulmonary metastatic tumors were divided into 5 groups of 3 mice each, consisting of 3 experimental groups (Hela, HepG2, and B16/F10 groups), 1 blocking group, and 1 control group. All groups were imaged by planar gamma.

In experimental groups, the mice received ^{99m}Tc-RRL (7.4 MBq, 100 μL [pH = 7.4]) and were imaged. ^{99m}Tc-RRL were purified and separated by on a Sephadex G25 gel filtration column. In the control group, mice were administered 7.4 MBq Na^{99m}TcO only, and in the blocking group 500 mg of unlabeled RRL was injected into each mouse 30 min before injection of ^{99m}Tc-RRL. All injections were successful with no leakage. The imaging time points were chosen based on our previous study [20], in which uptake was maximized. Whole-body planar imaging was performed 2 and 4 h after injection in the Department of Nuclear Medicine of Peking University First Hospital using a SPECT instrument (SPR SPECT; GE Healthcare, Inc., [Fairfield, Conn, USA]) equipped with a low-energy, high-resolution, parallel-hole collimator. Planar images were acquired at 200 k counts with a zoom factor of 2.0. The images were digitally stored in a 256×256 matrix size.

Statistical analysis

Statistical analysis was performed using one-way ANOVA analysis. The software used was SPSS 19.0. All results are expressed as the mean ± SD. A 95% confidence level was chosen to determine statistical significance, with a $P<0.05$ considered to be statistically significant.

Results

Biodistribution of ^{99m}Tc-RRL in pulmonary metastases mice

The bio-distribution data are shown in **Table 2** and **Figures 2** and **3**. The biodistribution of

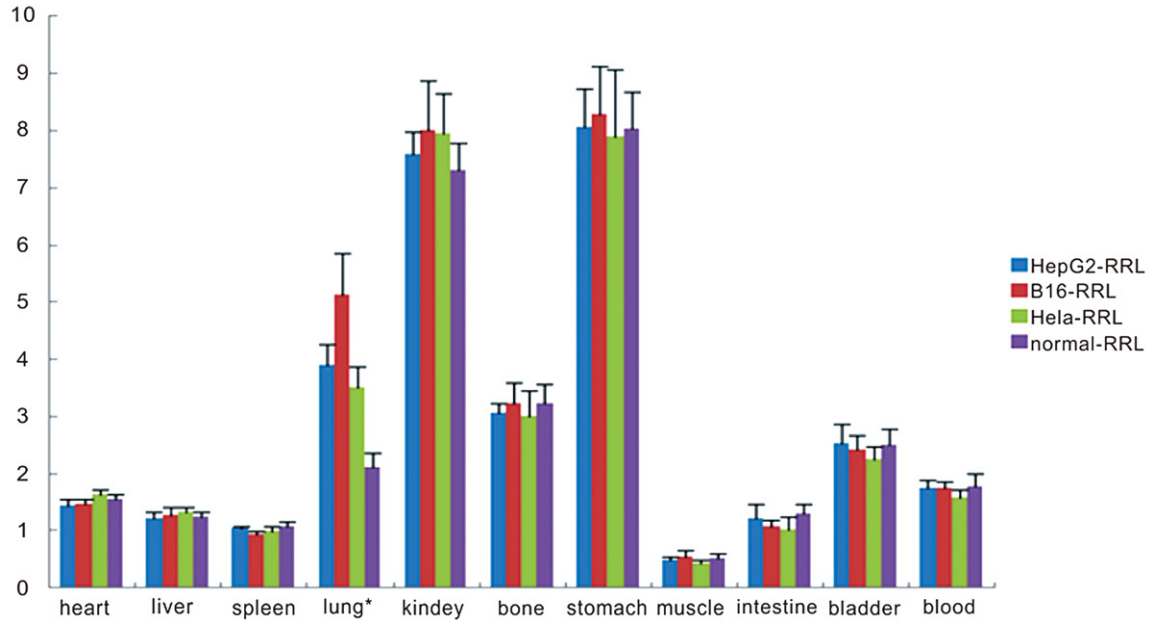

Figure 2. Bio-distribution of ^{99m}Tc-RRL in the HepG2, B16, and Hela pulmonary metastases models and in normal mice (4 h). Data are expressed as the mean ± SD (n = 4). The uptake by the lung in pulmonary metastasis mice is much higher than normal mice.

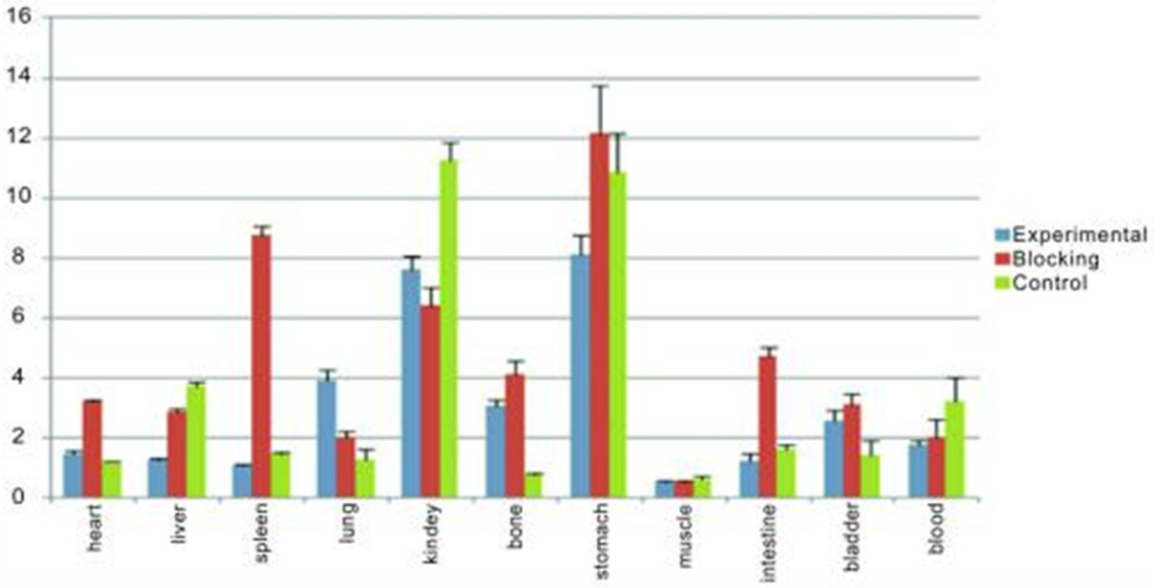

Figure 3. Bio-distribution of ^{99m}Tc-RRL in the HepG2 pulmonary metastasis model at 4 h. Comparison of % ID/g of organs of interest among experimental, blocking, and control groups 6 h post-injection is shown. Data are expressed as the mean ± SD (n = 4). The uptake by the lung in the pulmonary metastasis group is higher than by the blocking and control groups.

^{99m}Tc-RRL was determined in HepG2, B16, and Hela pulmonary metastases mice and compared with normal nu/nu mice 2 and 4 h after injection (**Table 2**), and the control and blocking groups 2 h after injection.

^{99m}Tc-RRL exhibited specific uptake values in the lungs of pulmonary metastases mice, and ^{99m}Tc-RRL also exhibited significantly higher lung uptake values in pulmonary metastases mice than normal mice ($P<0.05$; **Table 2**) 2 and

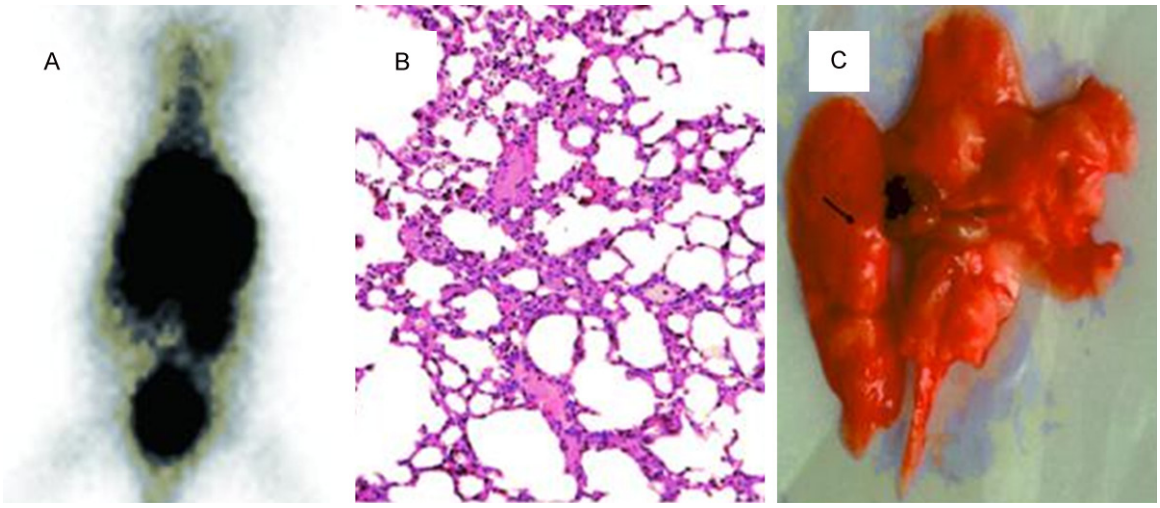

Figure 4. Planar imaging of pulmonary metastasis Hela-bearing mice. Images of the pulmonary metastases Hela model 2 h post-injection of the ^{99m}Tc-RRL are shown. The metastatic lesion in the lung is visible. (A) Immunohistochemical staining of the tumor, (B) HE staining of the tumor (×200) and (C) the dissected tumor specimen.

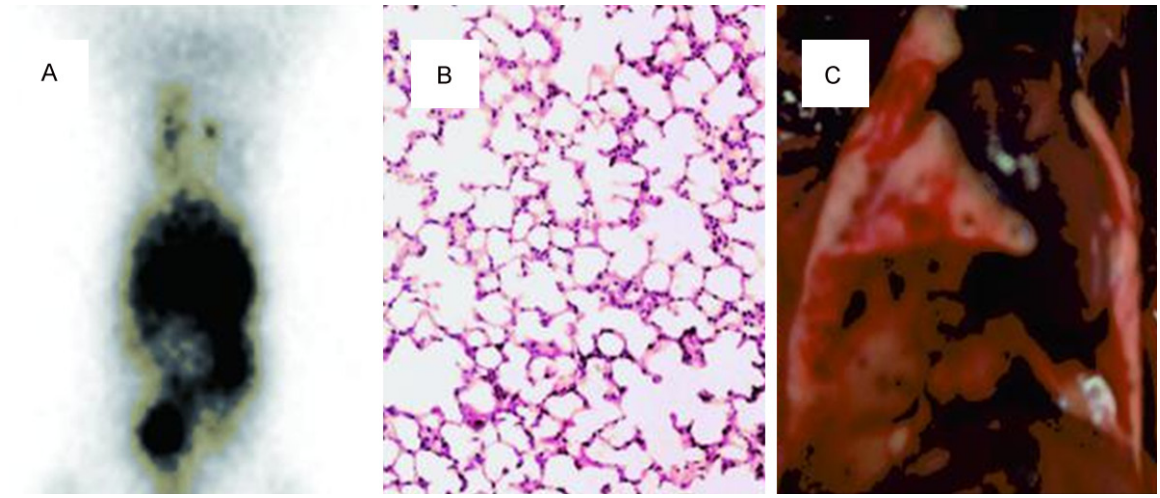

Figure 5. Planar imaging of the pulmonary metastasis B16-bearing model. Images of B16 pulmonary metastasis model 2 h post-injection of the ^{99m}Tc-RRL is shown. The metastatic lesions in the lung are visible. (A) Immunohistochemical staining of the tumor, (B) HE staining of the tumor (×200) and (C) the dissected tumor specimen.

4 h after injection. The lung uptake values were 3.92±0.48 and 3.89±0.36% ID/g in pulmonary metastases HepG2-bearing mice, 5.49±0.84 and 5.11±0.75 in % ID/g pulmonary metastases B16-bearing mice, 3.72±0.52 and 3.51±0.35% ID/g in pulmonary metastases Hela-bearing mice, and 2.38±0.20 and 2.11±0.24% ID/g in normal mice at 2 and 4 h, respectively. The ^{99m}Tc-RRL uptake values in the pulmonary metastases HepG2-bearing lungs were 1.65 and 1.84 times the lung uptake values in normal group 2 and 4 h after injection, respectively. The uptake values of the B16-bearing lungs were 2.31 and 2.42 times the values in normal mice at 2 and 4 h, respectively. The ^{99m}Tc-RRL uptake values in the Hela-bearing lungs were 1.56 and 1.66 times the values in normal mice at 2 and 4 h, respectively. ^{99m}Tc-RRL displayed higher lung-to-normal organ uptake ratios (rate of tumor/normal tissue) in the three pulmonary metastases mice compared with normal mice.

In the control group, uptake of the radiolabeled probe was similar to the experimental group in the blood, heart, spleen, muscle, and stomach ($P>0.05$). The data of tumor-bearing lung showed a significant difference between the experimental and control groups ($P<0.05$), but were similar to that of the blocking group ($P>0.05$). In the blocking group, the radiola-

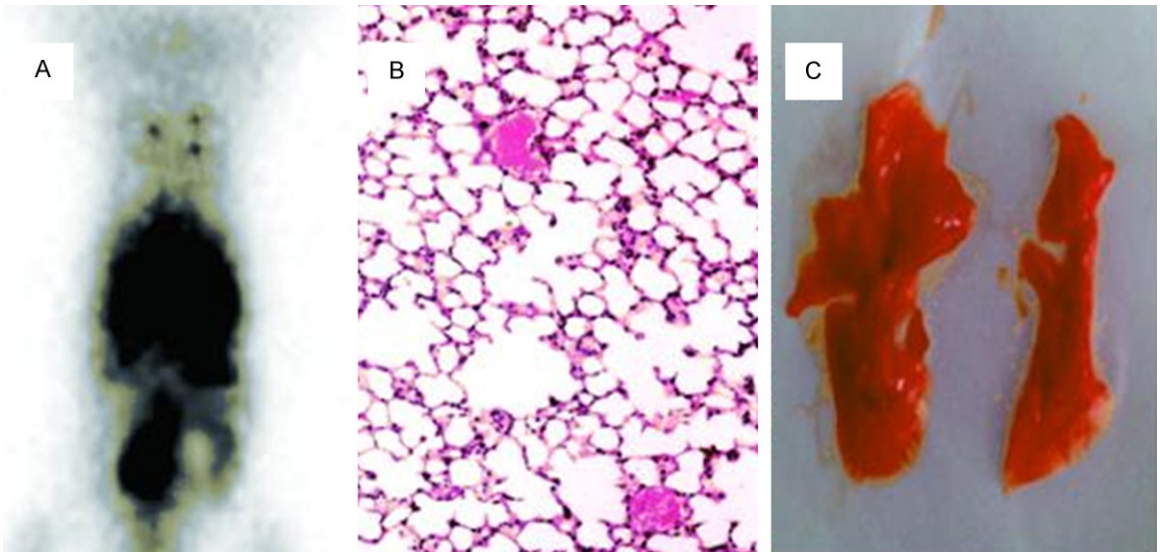

Figure 6. Planar imaging of the pulmonary metastasis HepG2-bearing model. Images of HepG2 pulmonary metastasis model 2 h post-injection of the ^{99m}Tc-RRL is shown. The metastatic lesions in the lung are visible. (A) Immunohistochemical staining of the tumor, (B) HE staining of the tumor (×200) and (C) the dissected tumor specimen.

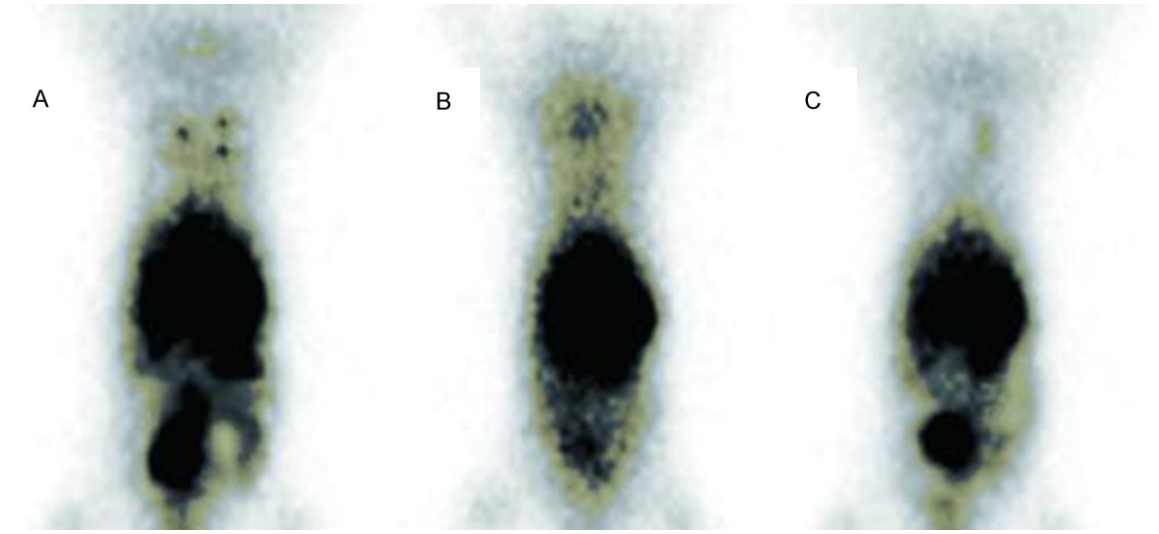

Figure 7. Comparison images of the pulmonary metastases HepG2-bearing models. In the blocking group immunohistochemical images, the tumors in the lung are not shown clearly at any time (B), but the experimental model shows clear uptake at 2 h (A). Control group also shows a vague imaging of the tumor (C).

beled probe had a greater distribution in the heart, spleen, stomach, and small intestine, but a lower distribution in tumor-bearing lung ($P<0.05$; **Figure 3**).

Planar imaging

Mice bearing different pulmonary metastatic tumors were injected with ^{99m}Tc-RRL through the tail vein to image metastatic deposits. Planar imaging data acquisition began 1 h after administration. The whole-body images of three different tumors are presented in **Figures 4**-**6**. The different pulmonary metastatic lesions were all clearly imaged after the administration of ^{99m}Tc-RRL. In the control and blocking groups, the tumors were not detected after injection of ^{99m}Tc-RRL at any time (**Figure 7**).

Detection of tumor by HE staining

The metastases were confirmed via necropsy after completion of the imaging study. The

results of hematoxylin/eosin staining are shown in **Figures 4-6**.

Discussion

We have previously reported that ^{99m}Tc-RRL can be used in the imaging of tumor xenografts. We now show that ^{99m}Tc-RRL can also be used to image pulmonary metastases and ^{99m}Tc-RRL can supplement ^{18}F-FDG PET imaging. We have demonstrated ^{99m}Tc-RRL imaging in three different pulmonary metastases models. Our data support the use of ^{99m}Tc-RRL to detect tumor metastases by targeting tumor angiogenesis.

In a previous study, Brown [21] first identified a tumor vasculature-specific binding peptide (RRL) using an *in vitro* bacterial peptide display library panned against tumor cells. *In vitro* binding experiments with tumor-derived epithelial cells (TDECs) were carried out. FITC-labeled RRL peptide showed the brightest staining and specificity for TDECs. Gregory [22] conjugated MBs to the peptide RRL via avidin/biotin bridging chemistry. MBs were successfully targeted to tumor-derived, but not normal endothelial cells. Our team then redesigned RRL and radiolabeled the peptide with ^{131}I. The bio-distribution of ^{131}I-RRL and *in vivo* imaging showed the potential of this imaging agent in BALB/c nude mice bearing PC3 human prostate carcinoma xenografts [23]. A further study confirmed that the adherence between RRL and different tumor cell lines, including B16, HepG2, and SKOV3, to be highly specific and this result was consistent with *in vivo* ^{131}I-RRL SPECT imaging. We concluded that it was unlikely that VEGFR-2 was the only binding ligand for tRRL targeted to tumor angiogenic endothelium, and suggested that radio iodinated tRRL can be a non-invasive method for functional molecular imaging of tumor angiogenesis [24]. In a subsequent study, Qian Zhao [20] radiolabeled the peptide with ^{99m}Tc and showed that ^{99m}Tc-RRL had potential as a molecular probe for imaging tumor angiogenesis in malignant liver carcinoma. Currently, many researchers are studying the visualization of cancer cell migration during the metastatic process [25-27], but few researchers have focused on imaging distant metastasis using radiolabeled agents. In the current study, we employed three different tumor cell models (B16, HepG2, and Hela), and demonstrated the visualization of distant metastasis using the novel probe, ^{99m}Tc-RRL.

As reported in our previous study [20], bio-distribution data in pulmonary metastases mice showed quick blood clearance, as most of the tracer was cleared within 4 h post-injection. In addition, the uptake rates of the tracer were determined in three types of tumor-bearing lungs. The lung uptake values and the times of tumor-bearing lung-to-normal lung were 3.89 and 1.84% ID/g in pulmonary metastases HepG2-bearing mice, 5.11 and 2.42% ID/g in B16-bearing mice, and 3.51 and 1.66% ID/g in Hela-bearing mice at 4 h, respectively. The bio-distribution data of ^{99m}Tc-RRL demonstrated that the lung uptake values in all pulmonary metastatic mice were significantly higher than normal mice ($P<0.05$). The above data demonstrate that ^{99m}Tc-RRL is a superb radiotracer for non-invasive imaging of pulmonary metastases. Compared with the experimental groups, the % ID/g value of tumor-bearing lung in the blocking group was significantly lower than that of the experimental group, and there was no statistically significant difference between the blocking and control groups ($P>0.05$). The bio-distribution results illustrated the specificity of ^{99m}Tc-RRL targeting tumors.

At present, the most commonly used contrast agent for cancer imaging is ^{18}F-fluorodeoxyglucose (^{18}F-FDG) because most tumors have characteristically high glucose metabolism. Unfortunately, pulmonary metastases may often be masked by surrounding inflammation and other benign lesions on ^{18}F-FDG imaging, making this method less effective in detecting pulmonary metastatic tumors clinically [28]; however, probes targeting tumor-induced angiogenesis, such as Arg-Gly-Asp (RGD), can avoid this shortcoming [29, 30]. Our study demonstrated rapid blood clearance and high tumor uptake of ^{99m}Tc-RRL, which was similar to the results on cyclic RGD in our previous study [20], and ^{99m}Tc-RRL has potential as a targeting probe for imaging tumor angiogenesis in malignant liver carcinoma. The ^{99m}Tc-RRL performance allowed the recognition of pulmonary and mediastinal metastases. The targeting probe, RRL, can complement the insufficiency of ^{18}F-FDG. Additionally, SPECT (single photon emission computed tomography) examination is much cheaper than PET (positron emission tomography). Examination by SPECT is more feasible for the treatment of patients with limited economic resources. These bio-distribution results show that the probe, ^{99m}Tc-RRL,

images pulmonary metastatic tumors, and can be used as a suitable supplement to ^{18}F-FDG imaging.

Three types of pulmonary metastatic lesions were clearly imaged using planar imaging with ^{99m}Tc-RRL. The images results corresponded to the bio-distribution results in pulmonary metastases (**Table 2**); however, not all individual metastatic foci were visible with ^{99m}Tc-RRL due to the resolution limitations of the instrument used. The metastases were confirmed on necropsy after completion of the imaging study. In the blocking imaging, the tumors were not shown after injection of ^{99m}Tc-RRL at any time. It was shown that the excess RRL blocked the radioactive uptake in tumor-bearing lungs, which illustrated specific affinity of the peptide with liver carcinoma. Images and bio-distribution data of ^{99m}Tc-RRL showed that the radiotracer also accumulated in the kidneys and stomach for the reasons mentioned previously [20], which may influence the imaging of abdominal tumors and metastases. To follow these results, our team could change the single peptide structure of RRL to solve this problem. In the current study, we investigated pulmonary metastases images and bio-distribution results, which indicated that ^{99m}Tc-RRL had the potential to be a candidate for imaging distant metastasis in the lung. Combined with our previous studies [20, 22, 23], ^{99m}Tc-RRL is a strong candidate imaging agent for specifically targeting tumor angiogenesis. RRL can successfully image both tumor xenografts and pulmonary metastases.

It is well known and established that the occurrence and final formation of metastasis is influenced by hypoxia and angiogenesis [31]. Imaging with ^{99m}Tc-RRL targeting tumor-induced angiogenesis can reveal the dynamics and sites of tumor angiogenesis, which could allow the guidance of anti-angiogenic drug therapy. Imaging plays a very important role in the management of patients with metastatic tumors. The timely identification of metastatic lesions can reduce patient morbidity and ultimately prolong survival. In the current study, pulmonary metastatic tumors could be imaged 8 weeks after cell injection. Future studies will be necessary to identify the minimal time within which imaging metastatic tumors is possible and to evaluate the capability of ^{99m}Tc-RRL in monitoring the progression of lung metastasis.

Conclusion

This bio-distribution and image study clearly demonstrated that ^{99m}Tc-RRL is an appropriate radiotracer for non-invasive imaging of pulmonary metastatic tumors. In combination with previous findings, we determined that ^{99m}Tc-RRL can image tumor xenografts and pulmonary metastatic tumors successfully. ^{99m}Tc-RRL targets tumor angiogenesis, thus allowing for SPECT molecular imaging and could serve as an adaptive complement to ^{18}F-FDG PET imaging in detecting metastatic tumors in the lung.

Acknowledgements

This work was supported by grants from the Natural Science Foundation of China (NSFC 30870729, 81071183) (http://www.nsfc.gov.cn/Portal0/default152. html), Ministry of Science and Technology of China (project 2011YQ030114 and 2011YQ03011409) (http://www.most.gov.cn/eng/); Research Fund for the Medicine and Engineering of Peking University (Fund BMU20120297) (http://en.coe.pku.edu.cn/); Research Fund Key Laboratory of Radiopharmaceuticals (Beijing Normal University), Ministry of Education, Department of Chemistry, Beijing Normal University, Beijing, China (120201) (http://radiopharm.bnu.edu.cn/); Fund for Key Projects in the National Science & Technology Pillar Program during the Twelfth Five-year Plan Period (2014BAA03B03) (http://www.most.gov.cn). The funders had no role in study design, data collection and analysis, decision to publish, or preparation of the manuscript.

Disclosure of conflict of interest

None.

Address correspondence to: Rong-Fu Wang, Department of Nuclear Medicine, Peking University First Hospital, No. 8, Xishenku Road, West District, Beijing, China. Tel: +86-010-83572914; Fax: +86-010-66551057; E-mail: rongfuwang89@163.com

References

[1] Saika K, Sobue T. Cancer statistics in the world. Gan To Kagaku RYOHO 2013; 40: 2475-2480.

[2] Kannivelu A, Loke KS, Kok TY, Osmany SY, Ali SZ, Suat-Jin L, Ng DC. The role of PET/CT in the evaluation of skeletal metastases. Semin Musculoskelet Radiol 2014; 18: 149-165.

[3] Borbely K, Nemeth Z, Kasler M. Clinical application of 18F-FDG PET/CT in the treatment of sarcomas. Magy Onkol 2014; 58: 24-31.
[4] Santoni M, Nanni C, Bittoni A, Polonara G, Paccapelo A, Trignani R, De Lisa M, Rychlicki F, Burattini L, Berardi R, Fanti S, Cascinu S. [(11) C]-methionine positron emission tomography in the postoperative imaging and follow up of patients with primary and recurrent gliomas. Isrn Oncol 2014; 463: 152.
[5] Belkic D, Belkic K. Molecular imaging in the framework of personalized cancer medicine. Isr Med Assoc J 2013; 15: 665-672.
[6] Tapan KN, Kayhan G, Diane EM, Martin WB. PET and MRI of metastatic peritoneal and pulmonary colorectal cancer in mice with human epidermal growth factor receptor 1-targeted 89Zr-labeled panitumumab. J Nucl Med 2012; 53: 113-120.
[7] Le Devedec SE, van Roosmalen W, Pont C, Lalai R, de Bont H. Two-photon intravital multicolour imaging to study metastatic behaviour of cancer cells in vivo. Methods Mol Biol 2011; 769: 331-349.
[8] Majzoub RN, Chan CL, Ewert KK, Silva BF, Liang KS, Jacovetty EL, Carragher B, Potter CS, Safinya CR. Uptake and transfection efficiency of PEGylated cationic liposome-DNA complexes with and without RGD-tagging. Biomaterials 2014; 35: 4996-5005.
[9] Durkan K, Jiang Z, Rold TL, Sieckman GL, Hoffman TJ, Bandari RP, Szczodroski AF, Liu L, Miao Y, Reynolds TS, Smith CJ. A heterodimeric [RGD-Glu-[(64)Cu-NO2A]-6-Ahx-RM2] αvβ3/GRPr-targeting antagonist radiotracer for PET imaging of prostate tumors. Nucl Med Biol 2014; 41: 133-139.
[10] Kunjachan S, Pola R, Gremse F, Theek B, Ehling J, Moeckel D, Hermanns-Sachweh B, Pechar M, Ulbrich K, Hennink WE, Storm G, Lederle W, Kiessling F, Lammers T. Passive versus active tumor targeting using RGD- and NGR-modified polymeric nanomedicines. Nano Lett 2014; 14: 972-981.
[11] Chaffer CL, Weinberg RA. A perspective on cancer cell metastasis. Science 2011; 331: 1559-1564.
[12] Fatemeh ZS, Behzad B, Fatemeh Z, Leili AM. Tumor angiogenesis and anti-angiogenic therapies. Human Antibodies 2013; 22: 15-19.
[13] Weidner N, Carol PR, Flax J, Blumenfeld W, Folkman J. Tumor angiogenesis correlates with metastasis in invasive prostate carcinoma. Am J Pathol 1993; 143: 401-409.
[14] Cook GJ. Pitfalls in PET/CT interpretation. Q J Nucl Med Mol Imaging 2007; 51: 235-243.
[15] Strauss LG. Fluorine-18 deoxyglucose and false-positive results: a major problem in the diagnostics of oncological patients. Eur J Nucl Med 1996; 23: 1409-1415.
[16] van Waarde A, Cobben DC, Suurmeijer AJ, Maas B, Vaalburg W, de Vries EF, Jager PL, Hoekstra HJ, Elsinga PH. Selectivity of 18F-FLT and 18F-FDG for differentiating tumor from inflammation in a rodent model. J Nucl Med 2004; 45: 695-700.
[17] McLarty K, Moran MD, Scollard DA, Chan C, Sabha N. Comparisons of [^{18}F]-1-deoxy-1-fluoro-scyllo-inositol with [^{18}F]-FDG for PET imaging of inflammation, breast and brain cancer xenografts in athymic mice. Nucl Med Biol 2011; 38: 953-959.
[18] Chen W. Clinical applications of PET in brain tumors. J Nucl Med 2007; 48: 1468-1481.
[19] Olivero WC, Dulebohn SC, Lister JR. The use of PET in evaluating patients with primary brain tumours: is it useful? J Neurol Neurosurg Psychiatry 1995; 58: 250-252.
[20] Zhao Q, Yan P, Wang RF, Zhang CL, Li L, Yin L. A novel 99mTc-labeled molecular probe for tumor angiogenesis imaging in hepatoma xenografts model: A pilot study. PLos One 2013; 8: e61043.
[21] Brown CK, Modzelewski RA, Johnson CS, Wong MK. A novel approach for the identification of unique tumor vasculature binding peptides using an E. coli peptide display library. Ann Surg Oncol 2000; 7: 743-749.
[22] Gregory ER, Michael KK, Ruth A. Ultrasonic imaging of tumor angiogenesis using contrast microbubbles targeted via the tumor-binding peptide arginine-arginine-leucine. Cancer Res 2005; 65: 533-539.
[23] Yu M, Zhou H, Liu X, Huo Y, Zhu Y, Chen Y. Study on biodistribution and imaging of radioiodinated arginine-arginine-leucine peptide in nude mice bearing human prostate carcinoma. Ann Nucl Med 2010; 24: 13-19.
[24] Lu X, Yan P, Wang R, Liu M, Yu M, Zhang C. The further study on radioiodinated peptide Arg-Arg-Leu targeted to neovascularization as well as tumor cells in molecular tumor imaging. J Radioanal Nucl Ch 2011; 290: 623-630.
[25] Zhang Y, Zhang W, Qin L. Mesenchymal-mode migration assay and antimetastatic drug screening with high-throughput microfluidic channel networks. Angew Chem Int Ed Engl 2014; 53: 2344-2348.
[26] Stoletov K, Kato H, Zardouzian E, Kelber J, Yang J, Shattil S, Klemke R. Visualizing extravasation dynamics of metastatic tumor cells. J Cell Sci 2010; 123: 2332-2341.
[27] Winnard PT Jr, Kluth JB, Kato Y, Artemov D, Raman V. Development of novel chimeric transmembrane proteins for multimodality imaging of cancer cells. Cancer Biol Ther 2007; 6: 1889-1899.
[28] Sampath L, Kwon S, Hall MA, Price RE, Sevick-Muraca EM. Detection of cancer metastases with a dual-labeled near-infrared/positron

emission tomography imaging agent. Transl Oncol 2010; 3: 307-317.
[29] Liu Z, Huang J, Dong C, Cui L, Jin X, Jia B, Zhu Z, Li F, Wang F. ^{99m}Tc-labeled RGD-BBN peptide for small-animal SPECT/CT of lung carcinoma. Mol Pharm 2012; 9: 1409-1417.
[30] Suri SS, Mills S, Aulakh GK, Rakotondradany F, Fenniri H, Singh B. RGD-tagged helical rosette nanotubes aggravate acute lipopolysaccharide-induced lung inflammation. Int J Nanomedicine 2011; 6: 3113-3123.
[31] Raghunand N, Gatenby RA, Gillies RJ. Microenvironmental and cellular consequences of altered blood flow in tumours. Br J Radiol 2003; 1: S11-22.